Received: 22 April 2025 | Revised: 28 August 2025 | Accepted: 5 September 2025

DOI: 10.1002/VIW.20250061

VIEW

RESEARCH ARTICLE

In situ monitoring of cell adhesion kinetics using label-free optical biosensors: Evaluating anticancer potential and selectivity of natural compounds

Beatrix Péter[1] | **Tim Ausbüttel**[2] | **Nicolett Kanyo**[1,3] | **Péter Joó**[1,3] | **Kinga Tóth**[1] | **Zoltán Szittner**[1] | **Inna Szekacs**[1] | **Szilvia Bosze**[4,5] | **Gábor M. Kovács**[6,7] | **Imre Boldizsár**[2,6,8] | **Robert Horvath**[1,9]

[1]Nanobiosensorics Laboratory, Institute of Technical Physics and Materials Science, HUN-REN Centre for Energy Research, Budapest, Hungary

[2]Department of Pharmacognosy, Semmelweis University, Budapest, Hungary

[3]Chemical Engineering and Material Sciences Doctoral School (CEMSDS), University of Pannonia, Veszprém, Hungary

[4]HUN-REN–ELTE Research Group of Peptide Chemistry, Institute of Chemistry, ELTE Eötvös Loránd University, Budapest, Hungary

[5]Department of Genetics, Cell- and Immunobiology, Semmelweis University, Faculty of Medicine, Budapest, Hungary

[6]Department of Plant Anatomy, Institute of Biology, Eötvös Loránd University, Budapest, Hungary

[7]Plant Protection Institute, Centre for Agricultural Research, Budapest, Hungary

[8]Center for Pharmacology and Drug Research & Development, Semmelweis University, Budapest, Hungary

[9]Institute of Biophysics, HUN-REN Biological Research Centre, Szeged, Hungary

Correspondence
Beatrix Péter
E-mail: peter.beatrix@ek.hun-ren.hu

Szilvia Bosze
E-mail: szilvia.bosze@ttk.elte.hu

Imre Boldizsár
E-mail: boldizsar.imre@ttk.elte.hu

Funding information
Hungarian Academy of Sciences (Lendület "Haladó" [Momentum Advanced] Program); TKP2021-EGA-04 program; OTKA K 142904; K-135712; PD 134195; János Bolyai Research Scholarship of the Hungarian Academy of Sciences; NKFIH University Research Scholarship Program 2025-2.1.1-EKÖP-2025-00025 of University of Pannonia; VEKOP-2.3.3-15-2017-00020;

Abstract

The limitations of conventional techniques hinder the identification of natural compounds with anticancer potential in terms of speed, throughput, sensitivity, and the capability of continuous monitoring of relevant biological effects. Novel label-free optical biosensors represent new opportunities in the discovery of drug candidates, eliminating these difficulties. Our study monitored the anti-adhesive effects of 11 isolated pure natural compounds (representing four different structural frameworks) and four crude extracts, obtained from plant and fungal sources. The resonant waveguide grating (RWG) method (using an evanescent field-based label-free optical biosensor) and a combined miniaturized holographic microscope technique were applied to investigate the effects of pure compounds and crude extracts on cancerous (HeLa) and healthy (pre-osteoblast) model cells in real time. The adhesion kinetics on fibronectin-coated surfaces and the morphological parameters on polystyrene surfaces were studied using these model cells in the presence and absence of compounds and extracts.

Beatrix Péter, Tim Ausbüttel, Imre Boldizsár and Robert Horvath contributed equally to this work.

National Research, Development, and Innovation Office (NKFIH), Grant/Award Numbers: ERC_HU, K-135712, KKP_19, OTKA K 142904, PD 134195, TKP2021-EGA-04, UniversityResearchScholarshipProgram-2025-2.1.1

The introduced biosensor method also investigated their interaction with the fibronectin surface. This methodology enables continuous, high-sensitivity parallel measurements, facilitating the identification of natural compounds with anticancer potential while also providing insights into their mechanism of action. The interaction of the aryltetralin lignans deoxypodophyllotoxin and angeloyl podophyllotoxin with fibronectin was confirmed as a key mechanism behind their non-selective anti-adhesive effects. In contrast, the selective adhesion inhibitory effects of the neolignan balanophonin and the alkaloid vermelhotin against HeLa cells were unrelated to fibronectin interaction.

KEYWORDS
adhesion kinetics, anticancer agents, cell adhesion, compound adsorption, fibronectin coating, natural compounds, optical label-free biosensor, selectivity

1 | INTRODUCTION

Natural small molecules play a crucial role in medicine, particularly cancer treatment.[1] From 1981 to 2019, 41% of all registered small-molecule anticancer drugs originated from natural sources.[2] These compounds provide a vast and largely untapped resource for developing novel, effective cancer therapies.

Label-free biosensors offer a powerful approach for screening natural compounds, enabling real-time, continuous monitoring of their effects on cellular processes.[3] Unlike conventional endpoint assays, label-free techniques allow for the dynamic assessment of cell adhesion, migration, and signaling in response to bioactive molecules.[4,5] This provides deeper insights into the mode of action of potential drug candidates and facilitates the identification of compounds with selective activity against cancer cells while sparing healthy ones. Despite these advantages, the widespread use of biosensors in natural compound screening remains limited. Challenges such as standardization, sensitivity optimization, and integration with high-throughput platforms need to be addressed to unlock their full potential. As biosensor technology advances, its application in drug discovery, particularly in screening nature-derived anticancer agents, could revolutionize the development of targeted and more effective therapies.[1,6–8]

Several lignan derivatives are represented among small-molecule anticancer drugs, such as etoposide and teniposide. They are semisynthetic derivatives of the highly toxic lignan podophyllotoxin, which can be isolated from various plant species. Podophyllotoxin can bind to tubulin, resulting in the inhibition of microtubule assembly during mitosis of cancer cells. While it is effective against cancer cells, it is also toxic to healthy cells. This highlights the necessity to identify additional related compounds that exhibit improved anticancer activity and reduced toxicity and investigate the mechanisms of action of these newly identified compounds.[9] The basic structure of lignans consists of two phenylpropane units, which are linked through the two β carbon atoms (C8 and C8') of their propyl groups (Figure 1). The neolignans also contain two phenylpropanes but are not C8–C8' linked. Lignans comprise several subgroups, including aryltetralin lignans and dibenzylbutyrolactone lignans. Dibenzylbutyrolactone lignans contain a γ-butyrolactone moiety, while the aryltetralin lignans, in addition to the C8–C8' bond, form another C–C bond between C2 and C7'. Podophyllotoxin derivatives are classified as aryltetralin lignans but also contain a γ-butyrolactone moiety. This results in a high structural similarity between the base structures of podophyllotoxin derivatives and dibenzylbutyrolactone lignans (see Figure 1).

Podophyllotoxin derivatives, that is, deoxypodophyllotoxin (DPT), 5′-demethoxydeoxypodophyllotoxin (demethoxy-DPT), and angeloyl podophyllotoxin (APT), and along with the dibenzylbutyrolactone anhydropodorhizol (AHP), have already been identified in the roots (DPT, APT, and AHP) and fruits (DPT and demethoxy-DPT) of *Anthriscus sylvestris* (L.) Hoffm.—cow parsley (Apiaceae). This herbaceous perennial plant has a strong taproot system and is commonly found in the Northern Hemisphere, providing a rich source of the lignans DPT, APT, and AHP. These lignans have also been confirmed as antiproliferative compounds.[9–13]

During adhesion processes, cells bind to the extracellular matrix (ECM) or other cells. Cell adhesion is crucial in cellular functions, including division, growth, movement, and differentiation. It is also essential in the spread of cancer cells. By inhibiting the adhesion of cancer cells, they lose their ability to interact with other cells and the surrounding environment, resulting in a decreased capacity to divide and metastasize. Cell movement plays a vital role

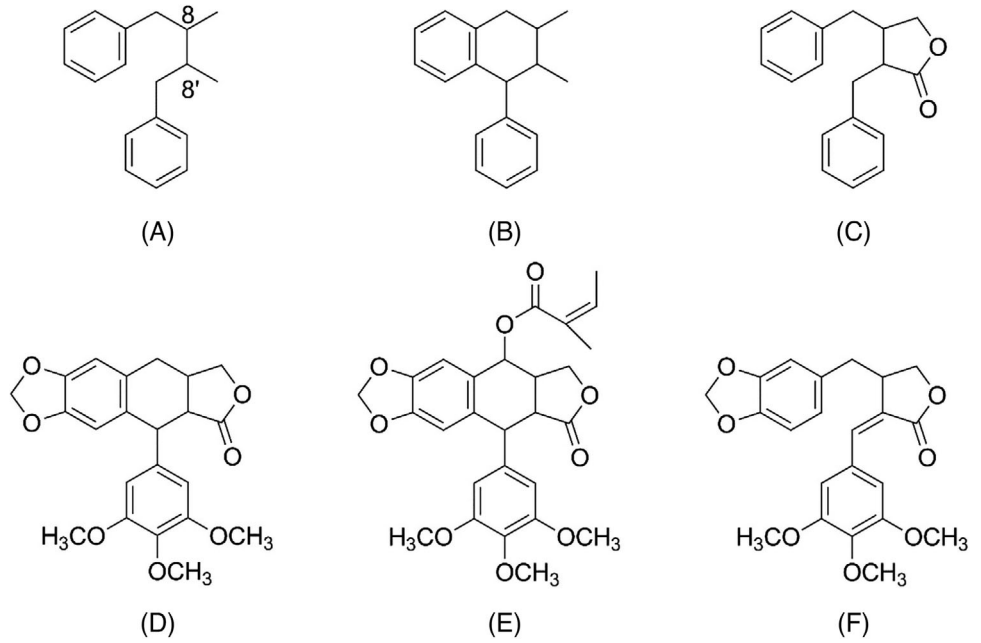

FIGURE 1 The basic structure of lignans (A), aryltetralin lignans (B), and dibenzylbutyrolactone lignans (C), along with the structures of the aryltetralin lignans deoxypodophyllotoxin (D) and angeloyl podophyllotoxin (E), as well as the dibenzylbutyrolactone lignan anhydropodorhizol (F).

in many biological processes, such as the adhesion of cells to each other and to the matrix, the functioning of the immune system, and wound healing.[5,14] Thus, cell adhesion and movement play a crucial role in the spread of cancer cells and the formation of metastases.

Fibronectin is a glycoprotein constituent of the ECM and a dissolved component of plasma (300 μg/mL) and other body fluids. Fibronectin is usually a dimer, consisting of the covalent connection of two nearly identical subunits of approximately 250 kDa. This glycoprotein plays a significant role in cell adhesion and tumor progression, making it an emerging target for the development of novel therapeutics.[15–17] As inhibition of adhesion is of particular importance in the mechanism of action of many anticancer agents, analyzing the effect of bioactive substances on cell adhesion to fibronectin coating can be an effective tool in identifying and designing novel anticancer drugs.[14,18–23]

Label-free optical methods, including resonant waveguide grating (RWG) and Holomonitor M4 transmission microscopy, enable the real-time analysis of living cell adhesion processes with high sensitivity, without affecting the cells through the addition of substances.[1,3] Among lignans, one aryltetralin lignan (a DPT derivative) and one dibenzylbutyrolactone lignan (enterolactone) have already been confirmed to reduce the adhesive ability of various cancer cells to fibronectin.[24,25] These results suggest that the antiproliferative effects of other lignans might also be related to their anti-adhesive properties.

We aimed to investigate how the adhesion processes of cancerous and healthy cells on a fibronectin coating are influenced by DPT, APT, and AHP, as well as by crude plant extracts containing these metabolites. To thoroughly assess the effect of these lignans on adhesion processes, our study also included three additional lignans, one neolignan, two caffeic acid (CA) derivatives, one alkaloid, and one coumarin, representing a variety of structurally different natural metabolites. Analyzing the effects of 11 well-defined natural metabolites and four crude extracts from various plant species on cell adhesion may contribute to the identification of potential antiproliferative drug candidates.

2 | MATERIALS AND METHODS

2.1 | Preparation of plant extracts for analysis using analytical high-performance liquid chromatography (HPLC) and label-free optical techniques, as well as for the isolation of lignans using preparative HPLC

The materials and reagents applied in the extraction, isolation, and analysis of compounds, such as acetonitrile, diethyl ether, distilled water, formic acid, methanol (Reanal, Hungary), and chlorogenic acid, were all of the analytical reagent grades of the highest purity available. Natural compounds trachelogenin,[26] pinoresinol, epipinoresinol,[27] balanophonin,[28] cichorin, acteoside, isoacteoside,[29] and vermelhotin[30] were isolated in our previous studies according to the indicated literature.

Plant material: Roots of *Anthriscus sylvestris* (L.) Hoffm. and *A. nitida* (Wahlenb.) Hazsl. (Apiaceae) were collected from different Hungarian locations in the flowering stage of the plants in May 2021. Sample collection locations of *A. sylvestris* and *A. nitida* were near Budapest (GPS, 47.540040, 18.971270) and near Felsőtárkány village (GPS, 47.991534, 20.458437), respectively. At least 10 individual plants were collected from both species. The roots of plants were pooled and lyophilized on the day of collection. The voucher specimens of the samples are deposited in the Department of Plant Anatomy, Eötvös Loránd University, Budapest, Hungary.

Lyophilized and pulverized root tissues of *A. sylvestris* and *A. nitida* (100.0 mg) were extracted with 20 mL of diethyl ether in 50-mL screw-capped vials at 60°C for 30 min. The insoluble, centrifuged material was then extracted twice as above. The combined supernatants were dried at 45°C in a standard vacuum rotary evaporator and referred to as crude diethyl ether extracts (CDEEs). After the CDEEs were prepared, the centrifuged root tissues, which had already been extracted with diethyl ether, were dried overnight at room temperature to remove any residual diethyl ether. The dried root tissues were extracted with 20 mL of methanol in 50-mL screw-cap vials at 60°C for 30 min. The insoluble, centrifuged material was then extracted twice using the same procedure as above. The combined supernatants were dried at 45°C in a standard vacuum rotary evaporator and referred to as crude methanol extracts (CMEEs).

2.2 | Isolation of lignans by preparative HPLC

The CDEEs were dissolved in 1.0 mL of methanol for the isolation of the lignans DPT, APT, and AHP by preparative HPLC using a Pharmacia LKB HPLC (Uppsala, Sweden) system (2248 pumps, VWM 2141 UV detector) connected to a preparative HPLC column: Gemini NX-C18 (5 μm), 25 × 1 cm (Phenomenex). Eluents: eluent A, 0.1% v/v formic acid, eluent B, acetonitrile:0.1% v/v formic acid (80:20, v/v). Gradient: 0.0 min, 30% B; 50.0 min, 100% B (linear gradient); 55.0 min, 100% B (linear gradient); flow rate: 5.0 mL/min; column temperature: ambient; injected volume: 500 μL.

2.3 | Identification and quantitation of compounds in the root extracts of *Anthryscus sylvestris* and *A. nitida* by analytical HPLC

Identification of compounds: The CDEEs, CMEEs, and the isolated compounds were dissolved in methanol. After preparing various dilutions with methanol, the diluted solutions were analyzed by a Dionex Ultimate 3000 HPLC system (3000RS diode array detector [DAD], TCC-3000RS column thermostat, HPG-3400RS pump, SRD-3400 solvent rack degasser, WPS-3000TRS autosampler) connected to an Orbitrap Q Exactive Focus Mass Spectrometer equipped with electrospray ionization (ESI) (Thermo Fisher Scientific). Gemini NX-C18 column (150 × 3 mm; 3 μm) (Phenomenex) was used for the process. Eluents used were as follows: eluent A, 0.1% v/v formic acid, eluent B, acetonitrile:0.1% v/v formic acid (80:20, v/v). Gradient program: 0.0 min, 20% B; 15.0 min, 90% B (linear gradient); 18.0 min, 90% B (isocratic). Flow rate: 0.4 mL/min; column temperature: 25°C; injected volume: 1.0–5.0 μL. The ESI source was operated in the positive and negative ionization mode (switching mode). Fragmentation was performed using the data-independent acquisition method with isolation widths of 100–300 *m/z*, 295–500 *m/z*, 495–800 *m/z*, and 795–1100 *m/z*, and collision energies of 15, 30, and 45 eV. The resolution for full and MS/MS scans was set to 70,000 and 17,500, respectively. Full MS scans were recorded in a 100–1500 *m/z* mass range. Ultraviolet (UV) spectra were collected between 230 and 400 nm, and UV chromatograms were generated by summing signal intensities within this wavelength range (other operation parameters were consistent with those described in our recent article).[31]

Quantification of compounds: An external standard method was employed using an HPLC-DAD technique. The total signal intensity of the DAD, measured in the wavelength range of 230–400 nm, was used to generate chromatograms (total scan mode). The HPLC parameters were identical to those described in the previous section, "Identification of compounds." Linear regression analyses of the isolated lignans (DPT, APT, and AHP) and standard chlorogenic acid were performed in the concentration range of 0.200–0.000823 mg/mL (DPT and AHP), 0.100–0.000823 mg/mL (APT), and 0.2440–0.0305 mg/mL (chlorogenic acid), resulting in the appropriate r^2 values (0.9974, DPT and AHP; 0.9981, APT; 0.9997, chlorogenic acid) (Figure S1).

2.4 | Cell cultures and cell adhesion assay buffer

Unless stated otherwise, all chemicals and reagents were obtained from Sigma-Aldrich Chemie GmbH.

HeLa cells (ECACC 93021013) were maintained in Dulbecco's modified Eagle's medium (31966021 Gibco), and MC3T3-E1 preosteoblast (ECACC 99072810) cells were maintained in α-modified minimal essential medium (32561029 Gibco), supplemented with 10% fetal bovine

serum (Gibco), 0.25 μg mL^{-1} amphotericin B, 100 U mL^{-1} penicillin, and 100 μg mL^{-1} streptomycin solution. Cells were cultured in a humidified incubator (37°C, 5% CO_2). On reaching 80% confluence, cells were detached every 3–4 days using 0.05% (w/v) trypsin and 0.02% (w/v) EDTA solution and were not used beyond passage 20.

The assay buffer was (20 mM 4-(2-hydroxyethyl)piperazine-1-ethanesulfonic acid (HEPES) in Hank's balanced salt solution (HBSS) (pH 7, hereafter HBSS-HEPES).

2.5 | Plant sample preparation for label-free optical analyses

The isolated pure compounds were dissolved in DMSO to prepare stock solutions at a concentration of 50 mM. The stock solutions were diluted with HBSS-HEPES buffer to prepare test solvents at a concentration of 200 μM, which were then serially diluted twofold with HBSS-HEPES until reaching a concentration of 6.25 μM.

The crude root extracts CDEEs and CMEEs were dissolved in 200 μL of DMSO. These solutions were 250-fold diluted with HBSS-HEPES buffer to prepare test solvents, which were then serially diluted twofold with HBSS-HEPES.

The serial dilutions of pure compounds and crude extracts were used in the label-free optical analyses.

2.6 | Resonant waveguide grating optical biosensor

We employed the Epic Benchtop (BT) system (Corning Incorporated), a RWG label-free optical biosensor. The Epic BT device can operate with 96- or 384-well standard Society for Biomolecular Screening format cell assay microplates. This label-free setup enables individual addressability of the sensors by utilizing a separate planar optical waveguide (made of niobium pentoxide) with a 2 × 2 mm optical grating at the bottom of each well. The Epic BT measures the resonant wavelength (λ) of each sensor every 3 s by tuning the uncoupled wavelength in the 825–840 nm range with a 0.25 pm precision. An optical waveguide enters an excited state on its resonant wavelength, in which any difference of the refractive index (RI) in the ~150 nm thick evanescent field above the surface of a sensor alters the resonant wavelength to a λ'-shifted resonant wavelength. As every biomolecule has an RI larger than that of water, their presence in the probing depth above the sensor surface causes RI changes. Processes such as dynamic cell mass redistributions, cellular spreading, or biomolecular surface adsorption can all lead to measurable RI variations. The Epic BT records the resonant wavelength shift ($\Delta\lambda = \lambda' - \lambda$), which is the difference between the shifted resonant wavelength (λ') and the resonant wavelength of the optical waveguide (λ).[17]

2.7 | Resonant waveguide grating optical biosensor measurements

A 384-well fibronectin-coated microplate (5042, Corning) was used for the biosensor measurements. Fibronectin coating procedure by the manufacturer: the microplate was coated by adding 10 μL per well of fibronectin solution (at 31.0 μg/mL) diluted with PBS. It was centrifuged for 10 s at 100 × *g*, and then incubated at room temperature for 1 h. After incubation, it was rinsed three times with PBS (50 μL per well) and dried on RT; the coated plate was stored in the fridge until the measurement was done. The measurements were performed in three parallel experiments (Figure 2A–F).

2.7.1 | Measurement steps for testing cell adhesion in the presence of isolated compounds and crude extracts

First, the baseline with HBSS-HEPES (30 μL) buffer was recorded. To eliminate bubbles, a centrifugation step was applied (100 × *g*, 10 s). The buffer was removed from the wells when the stable baseline was achieved in all biosensor wells. Various concentrations of the isolated compounds and multiple dilutions of the crude extracts, along with their corresponding control solutions, were pipetted into the appropriate wells (30–30 μL). We monitored the adsorption process for 90 min. In the next step, 12,000 cells (in 30 μL) were pipetted into the wells, and buffer was added to the wells without cells. We measured the process for 2 h. It should be noted that the concentration of the compounds and extracts was halved during the measurement due to the addition of the cell suspension.

2.7.2 | Measurement steps for testing cell adhesion after washing off the isolated compounds and crude extracts

The procedure is similar to the previous one, except that it includes a washing step after adding compounds and extracts. Compounds and extracts were allowed to adsorb onto the surface for 90 min. After adsorption, the wells were rinsed four times with 30 μL of assay buffer. Then, 30 μL of assay buffer was added to the wells, and signals were monitored for 90 min. In the next step, 12,000 cells/well

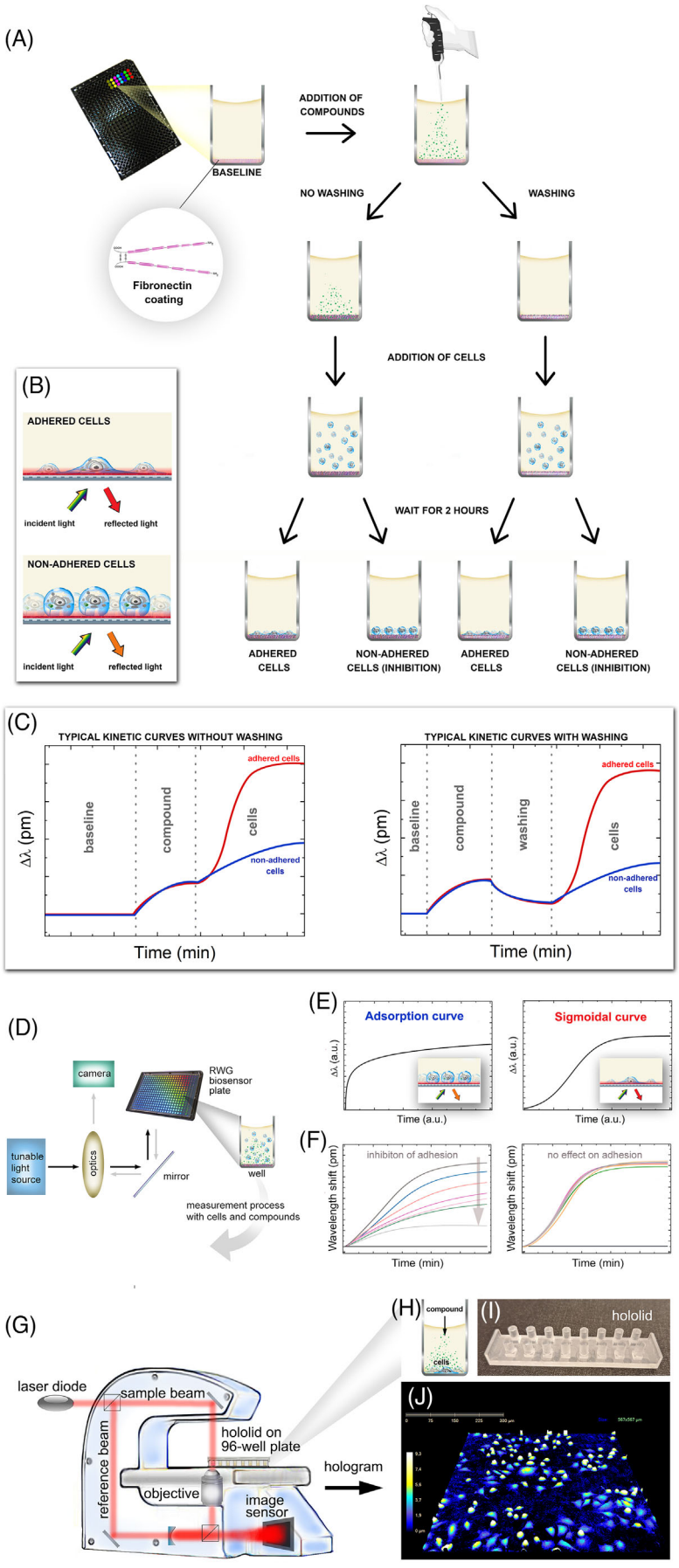

FIGURE 2 Schematic illustration of the multicomponent, continuous monitoring study measuring cell adhesion on a natural compound-treated coating. (A) A 384-well fibronectin-coated biosensor plate was used in the experiment (left), comprising the manipulation steps in a typical well (right). Representative kinetic curves are also shown (bottom). (B) The cells adhere to the fibronectin coating (upper image). The cell attaches but does not adhere to the biosensor surface (bottom image). The red zone represents the evanescent field. (C) Typical experimental curves are plotted without the washing procedure (left) and with the washing procedure (right). (D) Schematic illustration of the biosensor setup and sensor well. (E) Typical adhesion curves of the cells. Adsorption curves are plotted when the cells cannot adhere to the surface. They reach the evanescent field but cannot spread on the coating. Sigmoidal curves are plotted when the cells can adhere to the coating. (F) The compound inhibits cell adhesion in a concentration-dependent manner (reducing sigmoidal kinetic curves, left), while another compound does not affect cell adhesion (sigmoidal kinetic curves). (G) Working principle of the Holomonitor M4. (H) Schematic illustration of a 96-well plate well with adhered cells. (I) Photo of the used HoloLid. (J) Typical 3D images of the cells created by the Holomonitor technique (hologram).

were pipetted (30 µL) into the wells, and buffer was added to the wells without cells. We measured the process for 2 h.

2.7.3 | Measurement steps for testing the interaction of isolated compounds and crude extracts with fibronectin

First, the baseline with HBSS-HEPES (30 µL) buffer was recorded. To eliminate bubbles, a centrifugation step was applied (100 × *g*, 10 s). The buffer was removed from the wells when the stable baseline was achieved in all biosensor wells. Various concentrations of the isolated compounds and multiple dilutions of the crude extracts, along with their corresponding control solutions, were pipetted into the appropriate wells (30–30 µL). We monitored the adsorption process for 90 min.

2.8 | Holographic microscopy

The digital holographic microscopy Holomonitor M4 (Phase Holographic Imaging PHI AB) was used for label-free monitoring of the living cell adhesion process (Figure 2G–J). This high-resolution imaging technique provides real-time and quantitative measurements of cell physiology and morphology.[32–34] This method explores the phase shift of the probing laser light that has been reflected or transmitted through the monitored object. The phase shift is determined by the optical thickness of the sample, which depends on the RI inside the object and its physical thickness. The optical thickness can be measured with precision down to the nanometer scale.[35,36] HoloLid (Phase Holographic Imaging PHI AB) was used to prevent evaporation and ensure better image quality (Figure 2H–I). The manufacturer determined the setup of the Holomonitor and the HoloLid, and all guidelines were followed according to the manual.

2.9 | Holographic microscopy measurements

A 96-well uncoated tissue culture microplate (Sartstedt) was used for the measurement. A total of 25,000 cells in 150 µL of medium were pipetted into the wells and then incubated in the incubator at 37°C for 2 h, allowing the cells to adhere to the surface. Then, the medium was removed, and 100 µL of HBSS-HEPES and 100 µL of 200 µM isolated compound solutions, and 250-fold dilutions of crude extracts (in assay buffer) were added to the cells. The measurement lasted for 2 h; images of the wells were taken every 5 min. The measurement was recorded with the Hstudio M4 program (Figure 2J). Control measurements without compounds were also performed.

2.10 | MTT cell viability assay

At the confluent stage, cells were plated into 96-well tissue culture plates at an initial density of 5.0×10^3 cells per well. After 24 h, cells were treated with the compounds in serum-free medium containing 1.0% (v/v) DMSO at concentrations of 0.16, 0.8, 4, 20, and 100 µM. Control cells were treated with either serum-free medium alone or DMSO (1.0% v/v) under identical conditions. Following 3 h or overnight incubation, the cells were washed twice with serum-free medium. For cytotoxicity determination, the MTT solution was added at a final concentration of 0.37 mg/mL. For cytostasis determination, after washing, the cells were cultured for an additional 72 h in complete medium at 37°C. Next, the MTT solution (final concentration 0.37 mg/mL) was added to each well. The respiratory chain and other electron transport systems reduce MTT, forming non-water-soluble violet formazan crystals within the cells. After 3 h of incubation with MTT, the cells were centrifuged for 5 min at 900 *g*, and the supernatant was removed. The formazan crystals were then dissolved in 100 µL of DMSO, and the optical density (OD) was measured at 540 nm and 620 nm using an ELISA reader (iEMS Reader, Labsystems). OD620 values were subtracted from OD540 values. The amount of these crystals correlates with the number of mitochondria and, consequently, the number of living cells in the well. The percent of cytostasis was calculated using the following equation:

$$\text{Cytotoxic/Cytostatic effect (\%)} = 1 - (\text{OD treated}/\text{OD control}) \times 100 \quad (1)$$

where values OD treated and OD control represent the optical densities of the treated and control wells, respectively. In each case, two independent experiments were performed with four parallel measurements. The 50% inhibitory concentration (IC_{50}) values were calculated from the dose–response curves generated using Microcal Origin 2018 software. Cytostasis was plotted against concentration, and a sigmoidal curve was fitted to the data. Based on this curve, the IC_{50} value was determined and expressed in micromolar units.

3 | RESULTS AND DISCUSSION

3.1 | Determination of compounds in the crude extracts of *A. sylvestris*

The crude extracts of *A. sylvestris*, prepared by diethyl ether and methanol, CDEE, and CMEE, were analyzed by HPLC coupled with UV spectrophotometry and high-resolution tandem mass spectrometry (HR-MS/MS). The HPLC-UV

chromatogram of CDEE showed three main compounds. The molecular formulas calculated from the HR-MS data and the UV spectra of these compounds corresponded to those of the lignans DPT, AHP, and APT, which have already been identified in *A. sylvestris* (Figures S2 and S3).[37] This confirms that these lignans are also present in the CDEE and CMEE extracts. In addition to DPT, AHP, and APT, CMEE contained compounds with UV spectra comparable to those of CA derivatives (Figure S4). In the tandem mass spectra of these compounds, a high-intensity signal of the ions *m/z* 179 and *m/z* 161 can be observed corresponding to deprotonated CA and deprotonated CA after water loss (Figure S5). Based on these spectrometry results, we can confirm the presence of CA derivatives in the CMEEs, although their exact structures remain undetermined. Comparing the quantitative composition of the CDEE and CMEE, we found that the amounts of the lignans DPT, AHP, and APT were approximately 20 times higher in the CDEE than in the CMEE (Table S1). Additionally, the CA derivatives were present only in the CMEE. These results demonstrate that the lignans DPT, AHP, and APT can be selectively extracted using diethyl ether, enabling the preparation of extracts with a high lignan content. According to these findings, DPT, AHP, and APT were isolated from the CDEEs, and both extracts (CDEE and CMEE) were also tested to compare their anti-adhesive properties.

3.2 | Cell adhesion measurements by the RWG biosensor

To investigate the effects of DPT, AHP, and APT on adhesion processes using the RWG label-free optical biosensor technique, our study included crude extracts (CDEEs and CMEEs) of *A. sylvestris* that contained various amounts of these compounds, along with four additional lignans and four representatives of structurally different natural metabolites. We also prepared crude extracts from *A. nitida*, a plant species closely related to *A. sylvestris*, which is presumed to contain lignans, to test their effects on adhesion. These measurements using the RWG method and fibronectin coating were previously tested with epigallocatechin gallate (a catechin compound, Figure S6). As a result, this technique has been proven suitable for small-molecule research.[17]

3.2.1 | Cell adhesion in the presence of compounds

We previously confirmed that when cells cannot adhere to the surface, the kinetics of adhesion analyzed by the RWG biosensor show an adsorption-like curve.[38] In this case, the wavelength shift ($\Delta\lambda$) is also lower. Cell binding to the surface results in a sigmoidal-like adhesion kinetics curve. Therefore, when a compound inhibits cell adhesion, an adsorption-like kinetic curve can be observed with a lower $\Delta\lambda$ value rather than a sigmoidal-like kinetics curve characterized by higher $\Delta\lambda$ values. Typical measurement curves are shown in Figure 2E,F, representing this phenomenon.

In the present experiments, an active compound was considered to inhibit cell adhesion if it reduced cell adhesion to at least 80% compared to the control (Figure 3). The cell adhesion value cannot be zero because even in the case of non-adhering cells, they eventually reach the evanescent field. The strongest inhibitory effect observed in our measurements on HeLa and preosteoblast cells resulted in the lowest value, approximately 0.3 (Figure 3C). The effect of isolated compounds and crude extracts on the adhesion of HeLa cells and preosteoblasts is shown in Figure 3.

The isolated aryltetralin lignans DPT and APT exhibited adhesion inhibitory activity against HeLa cells and preosteoblast cells on fibronectin-coated surfaces (Figure 3A,B). The anti-adhesion effect of these compounds was not concentration dependent; even the lowest concentrations (3.125 and 6.25 μM) achieved a maximum inhibition of about 40%–50% against both cell types. The dibenzylbutyrolactone lignan AHP exhibited less significant anti-adhesive effects than the aryltetralin lignans DPT and APT (Figure 3A,B). However, AHP exhibited dose-dependent inhibition on both cell types, HeLa and preosteoblast, achieving maximal inhibitory activity at 50 μM. All dilutions of the crude diethyl ether extracts of *A. sylvestris* (AS-CDEE), which contain a mixture of DPT, APT, and AHP (Tables S1 and S2), demonstrated effectiveness against both cell types (Figure 3C,D). The concentration range of AHP in the diluted AS-CDEE samples was between 0.377 and 12.1 μM (Table S2). These values are much lower than the effective concentration of AHP required for maximal inhibition (50 μM), indicating that AHP does not significantly contribute to the efficacy of the AS-CDEE samples. Thus, the adhesion inhibitory activity of the AS-CDEEs may be related to their DPT and APT content. The crude methanol extract of *A. sylvestris* (AS-CMEE) contained DPT, APT, and AHP at approximately one-twentieth the levels found in AS-CDEE (as shown in Table S1). The AS-CMEEs demonstrated dose-dependent inhibitory activity within the dilution range of 16,000- to 4000-fold on HeLa cells, achieving maximal inhibition at the 4000-fold dilution (Figure 3C). The total amount of APT and DPT was only 0.141 μM in the 4000-fold dilution of AS-CMEE (Table S2; 0.108 μM DPT + 0.033 μM APT = 0.141 μM), representing the lowest concentration of these aryltetralin lignans that exhibited maximal inhibition. We included *A. nitida*, a plant closely

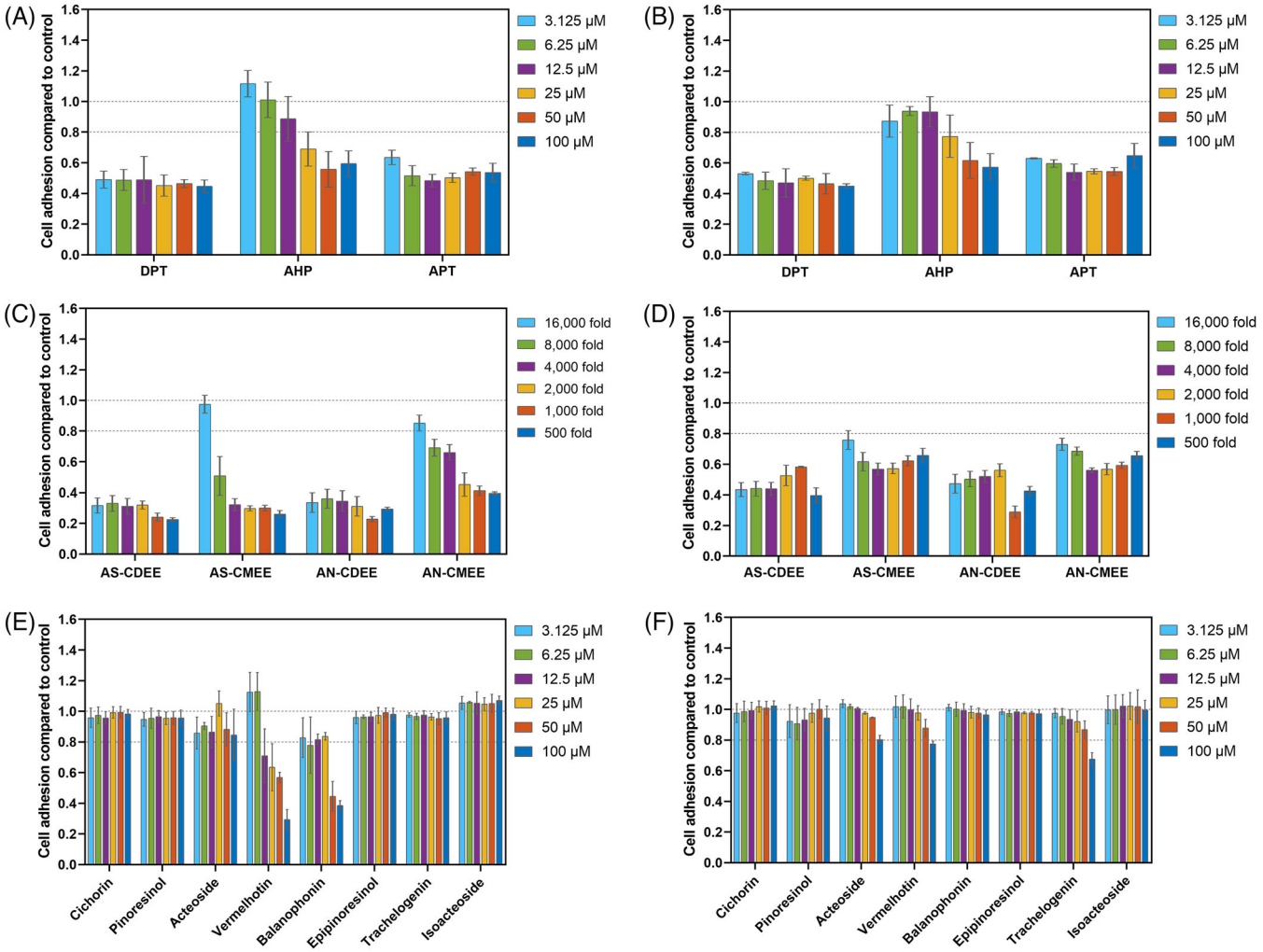

FIGURE 3 Effect of isolated compounds and crude extracts on the adhesion of HeLa (A, C, and E) and preosteoblast cells (B, D, and F). (A and B) The inhibitory effect of varying concentrations (3.125–100 µM) of deoxypodophyllotoxin (DPT), angeloyl podophyllotoxin (APT), and anhydropodorhizol (AHP) isolated from *A. sylvestris* on the adhesion of HeLa cells (A) and preosteoblast cells (B). (C and D) The inhibitory effect of various final dilutions (×500–×16,000) of crude diethyl ether extracts (CDEEs) and crude methanol extracts (CMEEs) prepared from *A. sylvestris* (AS-CDEE and AS-CMEE) and *A. nitida* (AN-CDEE and AN-CMEE) on the adhesion of HeLa cells (C) and preosteoblast cells (D). Treating concentrations of compounds in the various dilutions are in Table S2. This test did not utilize the 250-fold final dilution mentioned in Table S2. (E and F) The inhibitory effect of varying concentrations (3.125–100 µM) of the lignans pinoresinol, epipinoresinol, and trachelogenin; the neolignan balanophonin; the caffeic acid derivatives acteoside and isoacteoside; and the alkaloid vermelhotin on the adhesion of HeLa cells (E) and preosteoblast cells (F). Data represent ±SD ($n = 4$).

related to *A. sylvestris*, in the study, although its lignan content has not yet been analyzed. The crude extracts from *A. nitida*, prepared with diethyl ether and methanol (AN-CDEE and AN-CMEE), were also investigated for their adhesion inhibitory activity against HeLa cells (Figure 3C). The degree of inhibition induced by different dilutions of AS-CDEEs and AN-CDEEs, along with that of AS-CMEEs and AN-CMEEs, was similar, suggesting that adhesion-inhibiting compounds are also present in the crude extracts of *A. nitida*. The HPLC-UV-HR-MS analysis confirmed for the first time the presence of two aryltetralin lignans, DPT and demethoxy-DPT, and four dibenzylbutyrolactone lignans, as well as CA derivatives in the crude extracts of *A. nitida* (Figures S2–S5). The total amount of aryltetralin lignans in the same dilutions of AN-CMEE and AS-CMEE was comparable, suggesting that the adhesion-inhibiting activity of AN-CMEE may relate to its aryltetralin lignan content. As described above, the lowest total concentration of the aryltetralin lignans DPT and APT in AS-CMEE that exhibited maximal inhibition was 0.141 µM. The corresponding concentration value of the aryltetralin lignans DPT and demethoxy-DPT present in AN-CMEE was slightly higher (0.260 µM; in the 2000-fold dilution of AN-CMEE). These two inhibitory concentrations of aryltetralin lignans, which fall in the submicromolar range (i.e., 0.260 µM in AN-CMEE and 0.141 µM in AS-CMEE),

confirm their significant anti-adhesive activity against HeLa cells. The isolated aryltetralin lignans (DPT and APT) and crude extracts (AS-CDEE, AS-CMEE, AN-CDEE, and AN-CMEE) also expressed adhesion inhibitory activity against preosteoblast cells; however, this effect was not significantly concentration dependent (Figure 3B,D). We cannot rule out the possibility that other compounds in the crude extracts, such as dibenzylbutyrolactone lignans (found in CMEEs and CDEEs) and CA derivatives (present in CMEEs) (Table S2), may also affect the antiadhesive efficacy of aryltetralin lignans. To better understand the impact of DPT, APT, AHP, and crude extracts (CDEEs and CMEEs) on cell adhesion, we included eight additional compounds representing a variety of structurally distinct natural metabolites in our study (Figure 3E,F). The dibenzylbutyrolactone lignan (trachelogenin), which is closely related to AHP, two furofuran lignans (pinoresinol and epipinoresinol) bearing a bicyclic dioxygen framework, one neolignan (balanophonin) containing C8–C3′ linked phenylpropane units, and one alkaloid (vermelhotin) were also analyzed (Figure 3E,F). Trachelogenin was ineffective against HeLa cells, and only its highest concentration showed inhibition on preosteoblast cells, while pinoresinol and epipinoresinol were ineffective against both cell types. The neolignan balanophonin and the alkaloid vermelhotin inhibited the adhesion of HeLa cells without influencing preosteoblast cells. The CA derivatives, acteoside, isoacteoside, and coumarin cichorin showed no significant activity against either cell type (Figure 3E,F).

Given the inactivity of the CA derivatives acteoside and isoacteoside, we conclude that the related CA derivatives present in the CMEEs show little or no activity. Additionally, the dibenzylbutirolactone lignans, AHP, and trachelogenin were less effective as adhesion inhibitors, requiring concentrations above 50 μM. Furthermore, the related furofuran lignans, pinoresinol, and epipinoresinol were also ineffective. This indicates that dibenzylbutirolactone lignans have minimal or no contribution to the anti-adhesive effects of CMEEs and CDEEs. These results further support our conclusion that the aryltetralin lignans are the active compounds in these extracts.

3.2.2 | Adhesion of cells after washing off the compounds

The results of these tests did not clarify whether the adhesion inhibitory effect of the isolated compounds and crude extracts is achieved by directly impacting the cells or by binding to the fibronectin coating and blocking the relevant receptors.[17,19]

In the present experiment, we washed off the compounds from the fibronectin coating and monitored the subsequent cell adhesion to this treated and washed coating. Only those compounds were tested for their anti-adhesive effects after the washing procedure that demonstrated inhibitory effects against HeLa cells and/or preosteoblast cells in the previous tests without washing (i.e., the furofuran lignans pinoresinol and epipinoresinol, the coumarin cichorin, and the CA derivatives acteoside and isoacteoside were excluded from this study, while the neolignan balanophonin against HeLa cells, and the dibenzylbutyrolactone lignan trachelogenin against preosteoblast cells, were tested) (Figure 4A–D).

The adhesion inhibitory activity of all pure compounds was significantly lower after the washing procedure (Figure 4A,B) than without washing in both cell types, except for DPT, whose activity decreased minimally. As to the crude extracts of *A. sylvestris* (AS-CDEE, AS-CMEE) and *A. nitida* (AN-CDEE, AN-CMEE), containing mixtures of aryltetralin lignans and dibenzylbutyrolactone lignans, we can conclude that the washing procedure did not remarkably affect the activity of AS-CDEEs and AN-CDEEs in either cell type (Figure 4C,D). However, dilutions of AS-CMEE and AN-CMEE exhibited significantly reduced activity after washing in both cell types (Figure 4C,D). We described above that (1) the anti-adhesive effects of the crude extracts AS-CDEE and AS-CMEE correspond to their total DPT and APT content (Section 3.2.1), and (2) the total amount of DPT and APT were approximately 20 times higher in the AS-CDEE than in the AS-CMEE (Section 3.1), and (3) the washing procedure remarkably reduced the activity of APT and slightly decreased the activity of DPT (Figure 4A,B). Considering these results, we assume that the low aryltetralin lignan content in the AS-CMEE is reduced through washing to such an extent that it can exert only a lower inhibitory effect.

3.2.3 | Compound adsorption on fibronectin revealed by the RWG biosensor

We analyzed the adsorption properties of the isolated compounds and crude extracts to fibronectin. If the compound molecules reach the evanescent field, a wavelength shift is detected. The binding of molecules to the fibronectin coating was continuously monitored after they were added to the biosensor wells and after the subsequent washing procedure (i.e., pipetting buffer and then removing the solution several times). Typical kinetic curves of a well-adsorbing compound and those of poorly adsorbing compound are shown in Figure 4E,F.

When the adsorbed amount of a compound reaches a minimum 100 pm signal shift in terms of concentrations before the washing, it can be assumed that this compound

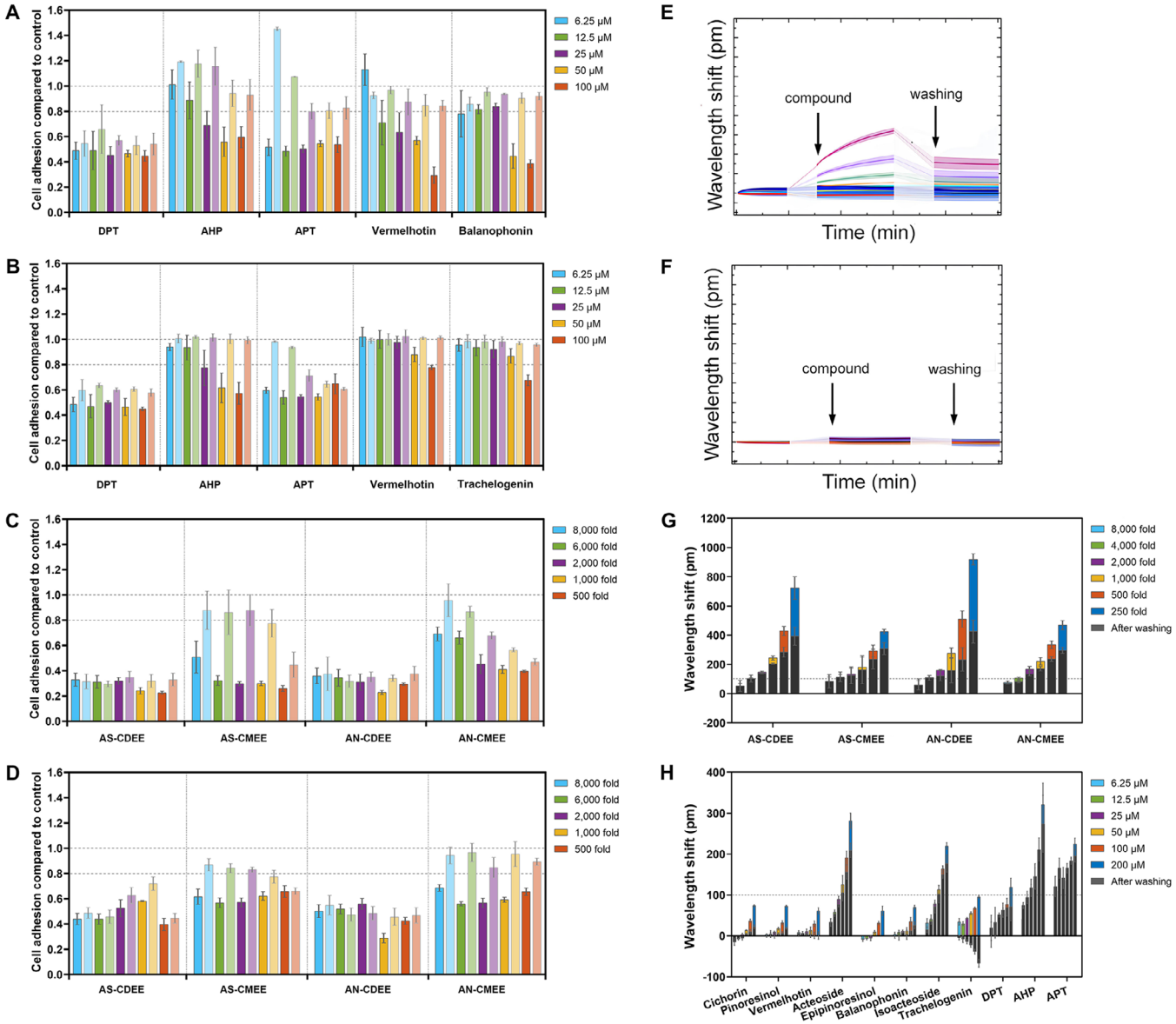

FIGURE 4 Comparison of the effect of the isolated compounds and crude extracts on the adhesion of HeLa and preosteoblast cells between the test method that includes a washing step and the test method that does not include a washing step (A–D), and the adsorption of the isolated compounds and crude extracts on fibronectin coating (E–H). (A and B) The inhibitory effect of varying concentrations (6.25–100 µM) of the isolated pure compounds deoxypodophyllotoxin (DPT), angeloyl podophyllotoxin (APT), anhydropodorhizol (AHP), vermelhotin, trachelogenin, and balanophonin on the adhesion of HeLa cells (A) and preosteoblast cells (B), determined without washing (dark columns) and after the washing procedure (bright columns). (C and D) The inhibitory effect of various final dilutions (×500–×8000) of crude diethyl ether extracts (CDEEs) and crude methanol extracts (CMEEs) prepared from *A. sylvestris* (AS-CDEE and AS-CMEE) and *A. nitida* (AN-CDEE and AN-CMEE) on the adhesion of HeLa cells (C) and preosteoblast cells (D), determined without washing (dark columns) and after the washing procedure (bright columns). (E) A typical curve of a compound that exhibits a very high level of adsorption (AS-CDEE). (F) Kinetic adsorption curve of a poorly adsorbing compound (pinoresinol). (G) Binding of various final dilutions (×250–×8000) of the crude extracts (AS-CDEE, AS-CMEE, AN-CDEE, and AN-CMEE) to fibronectin, determined without washing (colored columns) and after washing (black columns). (H) Binding of varying concentrations (6.25–200 µM) of the pure compounds DPT, APT, AHP, trachelogenin, pinoresinol, epipinoresinol, balanophonin, vermelhotin, cichorin, acteoside, and isoacteoside to fibronectin, determined without washing (colored columns) and after washing (black columns). Treating concentrations of compounds in the various dilutions of crude extracts are in Table S2. The final dilutions of 250-fold and 16,000-fold in the cell adhesion tests, as well as the 16,000-fold dilution in the fibronectin-binding tests, listed in Table S2, were not utilized. Data represent ±SD ($n = 4$).

has interacted with the fibronectin surface, and the amount of the absorbed molecules can be calculated[39] (Table S3). The compounds can interact with fibronectin in either a reversible or irreversible manner. The signal shift values measured after the washing step may correspond to the fraction of the compound irreversibly bound to fibronectin.

Before the washing step, the analysis of fibronectin-binding of isolated compounds and crude extracts showed that the adsorption signals increased significantly with increasing treatment concentrations (colored columns in Figure 4G,H). However, even at the highest concentrations, the isolated compounds cichorin, balanophonin, pinoresinol, epipinoresinol, trachelogenin, and vermelhotin did not reach the signal value of 100 pm, confirming their negligible or very weak binding to fibronectin. On the contrary, the crude extracts AN-CMEE, AN-CDEE, AS-CMEE, and AS-CDEE can interact with the fibronectin surface, as indicated by the RWG instrument, which detects extremely high signals exceeding 400 pm. The fibronectin-binding ability of the isolated compounds acteoside, isoacteoside, DPT, AHP, and APT is also supported by their signals exceeding 100 pm, at least at the highest concentration. By comparing the ratios of wavelength shifts detected before and after washing, it is evident that remarkable amounts of the isolated compounds and crude extracts with fibronectin-binding ability remain bound to fibronectin even after washing. This suggests that their interaction with fibronectin is likely irreversible. The strong fibronectin-binding ability of the CDEEs (AS-CDEE and AN-CDEE) may be attributed to their relatively high DPT, AHP, and APT content. In contrast, the significant fibronectin-binding capacity of the crude methanolic extracts (AS-CMEE and AN-CMEE), which contain only small amounts of these compounds, is likely due to the high values of CA derivatives structurally related to acteoside and isoacteoside.

The effects of isolated compounds and crude extracts on the adhesion of HeLa and preosteoblast cells to fibronectin-coated surfaces before and after washing (Figures 3 and 4A–D), as well as their interaction with fibronectin (Figure 4G,H), are summarized in Table 1.

The aryltetralin lignans DPT and APT showed significant inhibition of adhesion of cancer (HeLa) and healthy (preosteoblast) model cells without selectivity. The crude extracts containing DPT and APT (i.e., AS-CDEE, AS-CMEE, AN-CDEE, and AN-CMEE) also showed similar activity to that of pure DPT and APT. These isolated pure lignans and crude extracts exhibit strong interactions with fibronectin, suggesting that their effects on cell adhesion may be related to their binding to fibronectin. DPT is a more polar compound than APT, as also confirmed by their HPLC retention times: DPT eluted earlier than APT (Figure S3). This difference in polarity can be attributed to the presence of the highly apolar angeloyl group in APT, which may also influence their activity in relation to fibronectin binding. The neolignan balanophonin and the alkaloid vermelhotin were characterized as selective adhesion inhibitors of the cancerous HeLa cells without exhibiting any interaction with fibronectin. This indicates they may act directly on HeLa cells (Table 1, Figures 3 and 4A–D,G,H).

3.3 | Measurements with a holographic microscope

To study the potential direct effects of isolated compounds and crude extracts on adhesion processes, we investigated changes in adhesion and morphological parameters of cells using the Holomonitor M4 transmission microscopy method (Figure 5). This was done with HeLa cells attached to a polystyrene surface without a fibronectin coating. Following the treatments with isolated compounds and crude extracts, we assessed the changes in their adhesion (area of cells adhered to the surface and average optical thickness) and movement (migration, motility, and motility speed) behaviors. In the absence of adhesion, cells detach from the surface and roll up, resulting in a reduction in their surface area and, simultaneously, an increase in their average thickness, which the Holomonitor can detect. The isolated compounds DPT, APT, balanophonin, and vermelhotin, along with the crude extracts AS-CDEE, AS-CMEE, AN-CDEE, and AN-CMEE, which exhibited anti-adhesive effects on fibronectin coatings, were tested against HeLa cells. Preosteoblast cells were excluded from this study because previous results on fibronectin-coated surfaces indicated they were less sensitive to these compounds than HeLa cells (Figures 3 and 4). During the evaluation, 26–53 individual cells were tracked for 120 min following treatments with the isolated compounds and crude extracts. The treatment of HeLa cells with the neolignan balanophonin and the alkaloid vermelhotin resulted in a decrease in the surface area of the cells and an increase in their thickness. Figure 5A–E shows the changes in the morphology of the cells during the treatment time (5th, 60th, 120th min timepoints). Morphological changes are also shown in Figure S7. This confirms the adhesion inhibitory activity of balanophonin and vermelhotin against HeLa cells on polystyrene surfaces (Figure 5F–I). However, the aryltetralin lignans DPT and APT, along with the crude extracts AS-CDEE, AS-CMEE, AN-CDEE, and AN-CMEE, showed no effect on cell surface area or thickness (data not shown). Motility refers to the ability of a cell to move spontaneously and independently, which is measured by the actual distance the cell travels from its

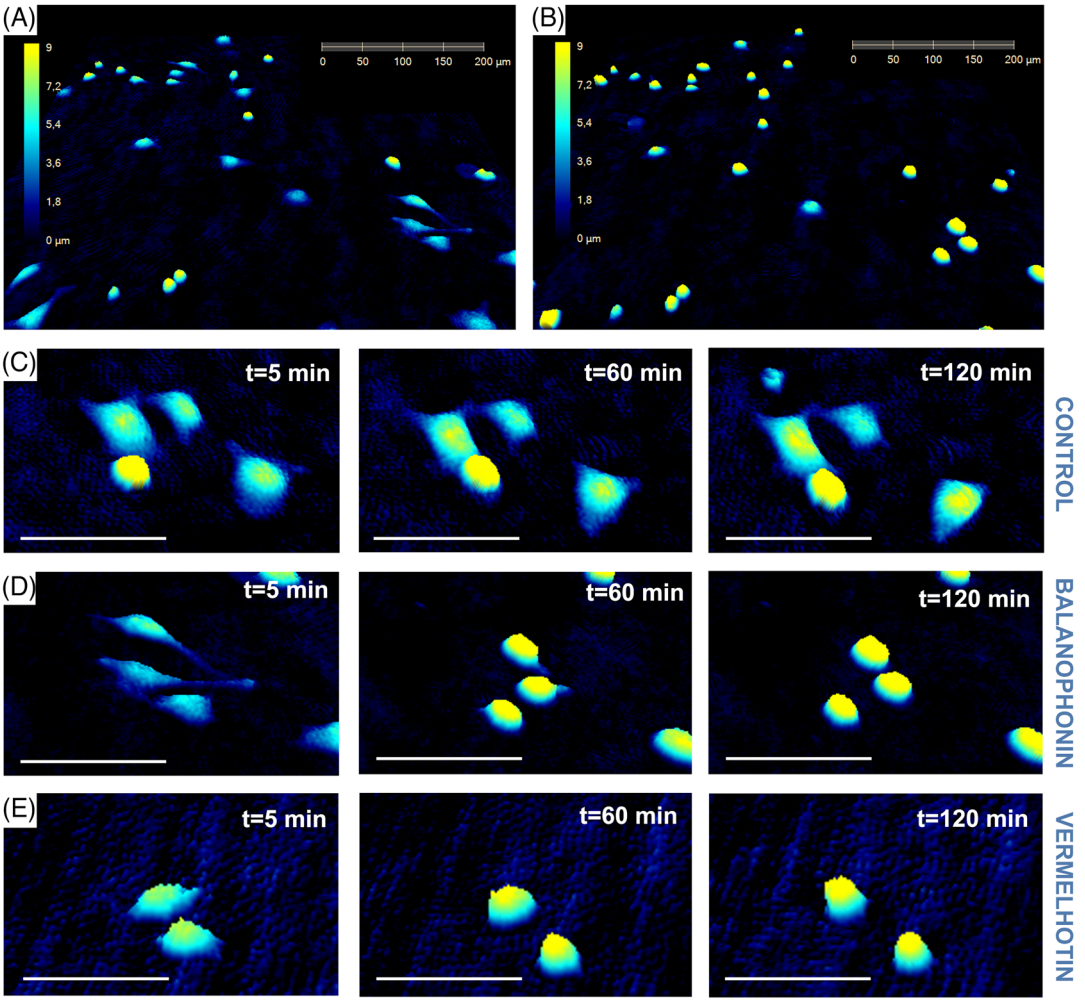

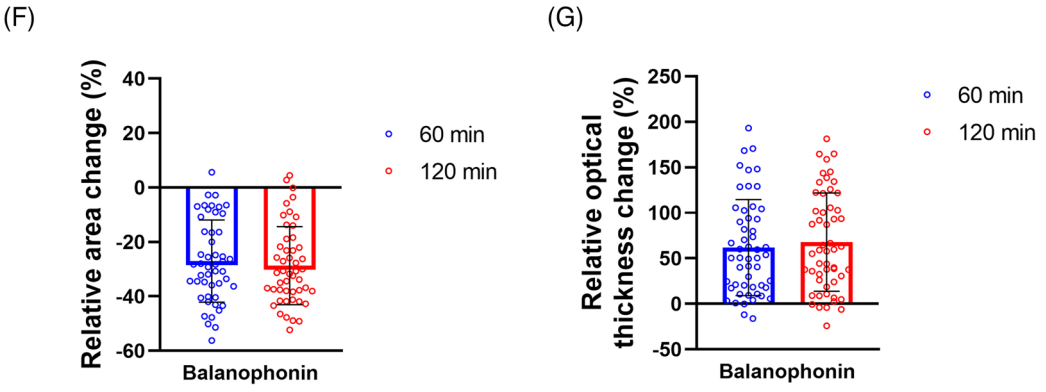

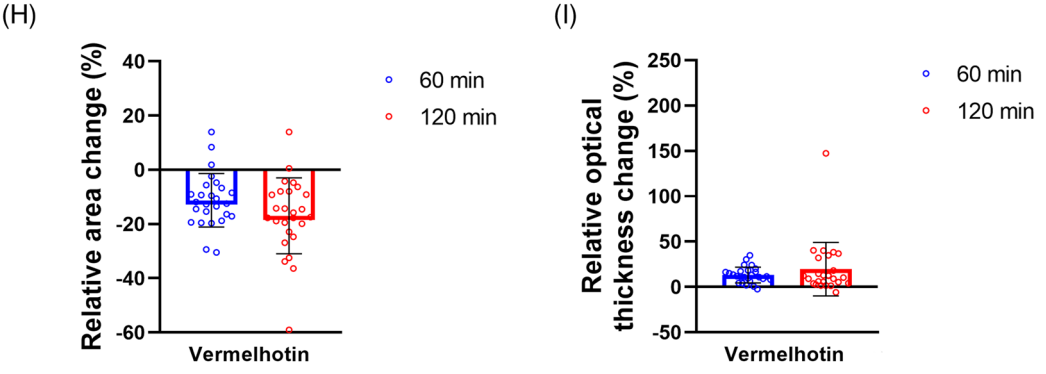

TABLE 1 Summary of the effects of isolated pure compounds and crude extracts on the adhesion of HeLa and preosteoblast cells to fibronectin-coated surfaces before and after washing and their interaction with fibronectin.

Type of compounds[a]	Compounds or crude extracts[b]	Inhibitory effects on cell adhesion[c]				Binding to fibronectin[d]
		HeLa cells		Preosteoblast cells		
		Without washing	With washing	Without washing	With washing	
ATL	DPT	+++	+++	+++	+++	Irreversible
	APT	+++	–	+++	+	Irreversible
DiBBL	AHP	++	–	++	–	Irreversible
ATL, DiBBL	AS-CDEE	+++	–	+++	–	Irreversible
	AN-CDEE	+++	–	+++	–	Irreversible
CA derivatives, ATL[e], DiBBL[e]	AS-CMEE	+++	+	+++	+	Irreversible
	AN-CMEE	++	+	+++	–	Irreversible
Neolignan	Balanophonin	++	–	–	NT	No
Alkaloid	Vermelhotin	++	–	–	–	No
CA derivatives	Acteoside	–	NT	–	NT	Irreversible
	Isoacteoside	–	NT	–	NT	Irreversible
Furofuran lignan	Pinoresinol	–	NT	–	NT	No
	Epipinoresinol	–	NT	–	NT	No
DiBBL	Trachelogenin	–	NT	+	–	No
Coumarin	Cichorin	–	NT	–	NT	No

[a]The isolated pure compounds and those identified in the crude extracts belong to the following metabolite groups: aryltetralin lignans (ATLs), dibenzylbutyrolactone lignans (DiBBLs), and caffeic acid (CA) derivatives.

[b]The isolated pure compounds—deoxypodophyllotoxin (DPT), angeloyl podophyllotoxin (APT), and anhydropodorhizol (AHP)—along with the crude diethyl ether extracts (CDEEs) and methanol extracts (CMEEs) from *A. sylvestris* (AS-CDEE and AS-CMEE) and *A. nitida* (AN-CDEE and AN-CMEE) were analyzed.

[c]The adhesion inhibitory effects were categorized as very strong (+++), strong (++), negligible (+), or ineffective (–). Compounds that showed no inhibitory activity against a cell type before washing were not tested (NT) for that cell type after washing.

[d]Compounds and extracts may exhibit negligible binding to fibronectin (denoted as NO) or remain bound to fibronectin after washing, indicating an irreversible interaction.

[e]ATLs and DiBBLs were determined as minor compounds in the crude extracts AS-CMEE and AN-CMEE.

starting point to the endpoint during the analysis. Migration means the shortest distance between the starting point and the endpoint. The tested compounds and extracts did not affect the motility or migration of HeLa cells (data not shown).

Considering the anti-adhesive activity of the isolated aryltetralin lignans DPT and APT, as well as the crude extracts AS-CDEE, AS-CMEE, AN-CDEE, and AN-CMEE on fibronectin-coated surfaces against HeLa cells—together with their strong interaction with fibronectin—and the absence of anti-adhesive effects on polystyrene surfaces without fibronectin, we suppose that their interaction with fibronectin plays a key role in their anti-adhesive activity (Figures 3–5, Table 1).

In contrast, the anti-adhesive effects of the neolignan balanophonin and the alkaloid vermelhotin against HeLa cells were independent of fibronectin interaction. Instead, their ability to inhibit adhesion is likely a direct effect on the cells, as they showed anti-adhesive activity on both fibronectin-coated and plain polystyrene surfaces without

FIGURE 5 Holomonitor 3D images and the analysis of the received data. The first (A) and the last (B) 3D images of the cells treated by balanophonin ($t = 5$ and 120 min). The cells rounded up, resulting in changes in the area and thickness parameters of the cells. (C–E) Typical morphological changes can be observed in the images of randomly selected and magnified cells at different time points ($t = 5$, 60, and 120 min). In the case of control (C), the cells remained almost the same during the measured time (2 h), however, after being treated with balanophonin (D), the cells rounded up. The change was less pronounced in the case of treatment with vermelhotin (E). (F–I) The graph represents the relative change in the cell area (μm^2) and the relative change in the averaged optical thickness (μm) expressed in percentages in the $t = 60$ and $t = 120$ min timepoints compared to the first timepoint of the measurement ($t = 5$ min) in the case of 100 μM balanophonin and vermelhotin treatment. (The number of tracked cells is in the case of control: 26, balanophonin treatment: 53, and vermelhotin treatment: 26.) The average data of the individual cells were used for analysis, and the standard deviation (SD) bars are also plotted in the graphs. (C–E) Scale bar: 100 μm.

TABLE 2 50% inhibitory concentration (IC_{50}) values of deoxypodophyllotoxin (DPT), angeloyl podophyllotoxin (APT), balanophonin, and vermelhotin on HeLa and preosteoblast cells.

	Cytotoxicity (IC_{50}, μM)				Cytostasis (IC_{50}, μM)			
	3 h		Overnight		3 h		Overnight	
Compound	HeLa	Preosteo blast	HeLa	Preosteo blast	HeLa	Preosteo blast	HeLa	Preosteo blast
DPT	>100	>100	0.2	10.2	>100	>100	0.2	0.4
APT	>100	>100	0.2	1.1	>100	>100	0.2	0.2
Balanophonin	>100	>100	10.5	20.5	>100	>100	20.4	9.9
Vermelhotin	>100	>100	15.6	30.2	>100	>100	21.9	26.8

demonstrating any fibronectin-binding ability. Of note, the adhesion-reducing effect is less significant in the case of vermelhotin compared to balanophonin measured by the Holomonitor technique.

3.4 | MTT assays on HeLa and preosteoblast (MC3T3-E1) cells

The compounds' in vitro cytotoxic and cytostatic effects were evaluated in both cell cultures. The IC_{50} values for the key active compounds, DPT, APT, balanophonin, and vermelhotin, were measured for both short (3 h) and long (24 h, overnight) periods to enable a comparative assessment of their efficacy and selectivity.

None of the compounds exhibits in vitro cytotoxic or cytostatic activities in both cell lines (HeLa and preosteoblast) after 3 h of treatment (in general, short incubation periods are used in RWG measurements). Therefore, it is important to note that cell viability remains largely unaffected within this timeframe.

However, as promising antitumor candidates, all compounds showed cytotoxic and cytostatic activity after 24 h (overnight) incubation on both cultures. Based on data from the endpoint type MTT assay (which measures mitochondrial enzyme activity related to cytotoxicity), balanophonin and vermelhotin exhibit very limited selectivity, as indicated by the IC_{50} values. However, the calculated selectivity index for both is greater than 2 (which is far from promising). Compounds DPT and APT have no selectivity after overnight incubation. Table 2 shows the exact data for the IC_{50} values.

Our data shows that after 3 h of incubation on the first screen, a promising group of compounds can be selected for further in vitro preclinical tests and different incubation times to evaluate their overall in vitro behavior profile.

It is important to note that selectivity can also be addressed later in drug development by using carrier systems specifically designed to enhance the candidate's selectivity through various strategies, depending on the area of investigation.

4 | CONCLUSIONS

Natural products present a dazzling array of chemical diversity that remains beyond the reach of synthetic chemistry. Each newly isolated and structurally or chemically characterized compound represents a potential opportunity for innovation. Notably, many of today's most widely used and still leading therapeutic agents are either of natural origin or are semi-synthetic derivatives thereof—essentially attempts to mimic nature. However, our ability to synthesize these complex structures is often limited and suboptimal. At the same time, a vast number of newly discovered compounds with novel and unexpected structures remain underexplored, primarily due to the lack of sufficient platforms for comprehensive biological testing. In our work, label-free biosensor techniques have proven valuable for rapidly screening isolated pure natural compounds and complex plant extracts containing diverse bioactive metabolites. The suggested methods are high throughput and label free, allowing continuous monitoring of cell–natural compound interactions in both healthy and cancerous cells. Using the developed methodology, we identified promising novel small-molecule candidates for further development as anticancer drugs. The RWG label-free optical biosensor and holographic microscopy confirmed that inhibiting cell adhesion is a significant mechanism by which the aryltetralin lignans, deoxypodophyllotoxin and angeloyl podophyllotoxin, exert their antiproliferative effects. Applying these methods to analyze plant extracts from *A. nitida*, a species not previously studied for its phytochemical composition, deoxypodophyllotoxin, and demethoxydeoxypodophyllotoxin were identified as anti-adhesive lignan constituents. However, we cannot exclude the possibility that other compounds present in the crude extracts, such as dibenzylbutyrolactone lignans and CA derivatives, may also contribute to or influence the antiadhesive efficacy of aryltetralin lignans. The adhesion inhibitory tests conducted with isolated compounds on cancerous (HeLa) and healthy (preosteoblast) model cells showed selective anti-adhesive activity of the alkaloid vermelhotin and the neolignan balanophonin toward cancerous HeLa cells.

The interaction of aryltetralin lignans with fibronectin was identified as a key mechanism underlying their non-selective anti-adhesive effects. Aryltetralin lignans such as podophyllotoxin derivatives have demonstrated various anti-cancer and anti-adhesive properties,[9,40,41] although direct inhibition of integrin-mediated adhesion has not been conclusively reported. Therefore, we hypothesize that the anti-adhesive effect of these compounds may involve interference with fibronectin-integrin recognition, potentially at the RGD-binding interface, or through modulation of integrin activity or membrane distribution. Moreover, interference with focal adhesion complex components (e.g., talin, paxillin, or focal adhesion kinase [FAK]) could be an alternative mechanism, given the central role of these proteins in integrin-cytoskeleton coupling.[42]

In contrast, the selective antiproliferative effects of balanophonin and vermelhotin were found to be independent of fibronectin interaction. We may assume that balaphonin and vermelhotin molecules bind to integrins, which are overexpressed or dominant in HeLa cells (e.g., $\alpha v\beta 5$),[43] thus they cannot reach the RGD motifs, resulting in selective adhesion inhibitory effects. However, they may inhibit cell adhesion via suppressing dominant "HeLa type" integrin expression as well as the membrane lipid raft-associated integrin function and downstream integrin signalling pathways (e.g., FAK).[42,44]

Adhesion dynamics are influenced by various factors, including integrin profiles, membrane glycosylation, and the cellular microenvironment, all of which can vary widely between cell types. Therefore, while the observed trends in adhesion modulation by natural compounds may indicate potential anticancer activity, further validation across a panel of cancer cell lines and relevant primary cells is necessary. Such comparative studies would help establish whether the detected biosensor responses are broadly applicable or cell-type specific, ultimately informing the translational relevance of the findings.

Label-free biosensors are suited to extracellular binding interactions or surface-level adhesion, but do not probe intracellular mechanical changes or force distributions directly. Combining with other new techniques, which are capable of detecting cellular mechanical force for quantifying cell viability after drug treatment, such as nano-electroporation-DNA tensioner platform,[45] can be a simple and powerful new system for clinical drug screening and development.

The aim of the present study was to establish and demonstrate a rapid screening method for assessing anti-adhesion effects, rather than to investigate detailed molecular interactions or downstream signaling pathways. Accordingly, experiments such as receptor binding assays or pathway-specific inhibition analyses were beyond the scope of this work. We believe these questions merit a dedicated follow-up study that builds upon the methodology introduced here. In conclusion, this study underscores the potential of label-free biosensor-based screening techniques in identifying natural compounds with anticancer potential rapidly and cost-effectively.

AUTHOR CONTRIBUTIONS

Beatrix Péter, Imre Boldizsár, and Szilvia Bosze conceived and designed the study and methodology, conducted experiments, and drafted and edited the manuscript. Tim Ausbüttel, Nicolett Kanyó, and Kinga Tóth performed the experiments. Péter Joó performed data curation and analysis. Inna Szekacs, Zoltán Szittner, and Gábor M. Kovács contributed to manuscript editing. Robert Horvath, Imre Boldizsár, Gábor M. Kovács, and Szilvia Bosze provided resources and technical support, supervised the project and oversaw administration. Beatrix Péter, Péter Joó, Imre Boldizsár, and Szilvia Bosze created the figures. Beatrix Péter, Imre Boldizsár, and Szilvia Bosze revised the manuscript. All the authors read and approved the final version.

ACKNOWLEDGMENTS

This research was funded by the Hungarian Academy of Sciences (Lendület "Haladó" [Momentum Advanced] Program), the National Research, Development, and Innovation Office (NKFIH) (ERC_HU, and KKP_19 Programs), TKP2021-EGA-04 program, K-135712 (to I.B.), OTKA K 142904 (to S.B.), and the PD 134195 (to Z.S.). This paper was supported by the János Bolyai Research Scholarship of the Hungarian Academy of Sciences (to B.P. and Z.S.), the NKFIH University Research Scholarship Program 2025-2.1.1-EKÖP-2025-00025 of University of Pannonia (to N.K.), and VEKOP-2.3.3-15-2017-00020 (to I.B., G.M.K., and S.B.).

CONFLICT OF INTEREST STATEMENT

The authors declare no conflict of interest.

ORCID

Beatrix Péter https://orcid.org/0000-0001-5601-2180
Robert Horvath https://orcid.org/0000-0001-8617-2302

REFERENCES

1. B. Péter, I. Boldizsár, G. M. Kovács, A. Erdei, Z. Bajtay, A. Vörös, J. J. Ramsden, I. Szabó, S. Bősze, R. Horvath, *Biomedicines* **2021**, *9*, 1781.
2. D. J. Newman, G. M. Cragg, *J. Nat. Prod.* **2020**, *83*, 770.
3. B. Péter, I. Szekacs, R. Horvath, *Heliyon* **2024**, *10*, e25603.
4. K. Kliment, I. Szekacs, B. Peter, A. Erdei, I. Kurucz, R. Horvath, *Biosens. Bioelectron.* **2021**, *191*, 113469.
5. I. Szekacs, N. Orgovan, B. Peter, B. Kovacs, R. Horvath, *Sens. Actuators B: Chem.* **2018**, *256*, 729.

6. B. G. Andryukov, N. N. Besednova, R. V. Romashko, T. S. Zaporozhets, T. A. Efimov, *Biosensors* **2020**, *10*, 11.
7. Y. Fang, *Drug Discov Today Technol.* **2011**, *7*, e5.
8. R. La Spina, V. E. V. Ferrero, V. Aiello, M. Pedotti, L. Varani, T. Lettieri, L. Calzolai, W. Haasnoot, P. Colpo, *Biosensors* **2018**, *8*, 1.
9. Z. Shah, U. F. Gohar, I. Jamshed, A. Mushtaq, H. Mukhtar, M. Zia-UI-Haq, S. I. Toma, R. Manea, M. Moga, B. Popovici, *Biomolecules* **2021**, *11*, 603.
10. T. Golakoti, H. K. Kancharla, B. Meka, Y. L. N. Murthy, *Med. Chem. Res.* **2016**, *25*, 2906.
11. C. Miranda-Vera, Á. P. Hernández, P. García-García, D. Díez, P. A. García, M. Á. Castro, *Pharmaceutics* **2023**, *15*, 2728.
12. P. Strus, K. Sadowski, W. Ploch, A. Jazdzewska, P. Oknianska, O. Raniszewska, I. Mlynarczuk-Bialy, *Int. J. Mol. Sci.* **2025**, *26*, 958.
13. R. Ikeda, T. Nagao, H. Okabe, Y. Nakano, H. Matsunaga, M. Katano, M. Mori, *Chem. Pharma. Bull.* **1998**, *46*, 871.
14. T. Okegawa, R. C. Pong, Y. Li, J. T. Hsieh, *Acta Biochim. Pol.* **2004**, *51*, 445.
15. R. Pankov, K. M. Yamada, *J. Cell Sci.* **2002**, *115*, 3861.
16. J. P. Wang, A. Hielscher, *J. Cancer* **2017**, *8*, 674.
17. B. Peter, N. Kanyo, I. Szekacs, A. Csampai, S. Bosze, R. Horvath, *Mater. Adv.* **2022**, *3*, 8684.
18. A. A. Khalili, M. R. Ahmad, *Int. J. Mol. Sci.* **2015**, *16*, 18149.
19. B. Peter, E. Farkas, E. Forgacs, A. Saftics, B. Kovacs, S. Kurunczi, I. Szekacs, A. Csampai, S. Bosze, R. Horvath, *Sci. Rep.* **2017**, *7*, 42220.
20. V. Srivastava, A. S. Negi, J. K. Kumar, M. M. Gupta, S. P. S. Khanuja, *Bioorg. Med. Chem.* **2005**, *13*, 5892.
21. W. H. Talib, A. M. Mahasneh, *Sci. Pharma.* **2010**, *78*, 33.
22. J. Yayan, K.-J. Franke, M. Berger, W. Windisch, K. Rasche, *Mol. Biol. Rep.* **2024**, *51*, 165.
23. K. T. Yip, X. Y. Zhong, N. Seibel, S. Pütz, J. Autzen, R. Gasper, E. Hofmann, J. Scherkenbeck, R. Stoll, *Sci. Rep.* **2016**, *6*, 25119.
24. L. Bai, R. Wang, Y. Zou, G. Xu, *Chem. Res. Chin. Univ.* **2015**, *31*, 964.
25. J. Chen, L. U. Thompson, *Breast Cancer Res. Treat.* **2003**, *80*, 163.
26. Z. Mervai, A. Sólyomváry, G. Tóth, B. Noszál, I. Molnár-Perl, K. Baghy, I. Kovalszky, I. Boldizsár, *Fitoterapia* **2015**, *100*, 19.
27. A. Sólyomváry, Á. Alberti, A. Darcsi, R. Könye, G. Tóth, B. Noszál, I. Molnár-Perl, L. Lorántfy, J. Dobos, L. Őrfi, S. Béni, I. Boldizsár, *J. Chromatogr. B* **2017**, *1052*, 142.
28. A. Sólyomváry, G. Tóth, B. Komjáti, P. Horváth, M. Kraszni, B. Noszál, I. Molnár-Perl, I. Boldizsár, *Process Biochem.* **2015**, *50*, 853.
29. M. Zürn, G. Tóth, M. Kraszni, A. Sólyomváry, Z. Mucsi, R. Deme, B. Rózsa, B. Fodor, I. Molnár-Perl, K. Horváti, S. Bősze, B. Pályi, Z. Kis, S. Béni, B. Noszál, I. Boldizsár, *Ind. Crops Prod.* **2019**, *139*, 111517.
30. P. J. Berek-Nagy, G. Tóth, S. Bősze, L. B. Horváth, A. Darcsi, S. Csíkos, D. G. Knapp, G. M. Kovács, I. Boldizsár, *Phytochemistry* **2021**, *190*, 112851.
31. G. Tóth, K. Horváti, M. Kraszni, T. Ausbüttel, B. Pályi, Z. Kis, Z. Mucsi, G. M. Kovács, S. Bősze, I. Boldizsár, *J. Nat. Prod.* **2023**, *86*, 672.
32. Á. G. Nagy, I. Székács, A. Bonyár, R. Horvath, *Sci. Rep.* **2022**, *12*, 10111.
33. Á. G. Nagy, I. Székács, A. Bonyár, R. Horvath, in 2020 43rd International Spring Seminar on Electronics Technology (ISSE), **2020**.
34. B. Peter, J. Nador, K. Juhasz, A. Dobos, L. Korosi, I. Székács, D. Patko, R. Horvath, *JBO* **2015**, *20*, 067002.
35. E. Mihaylova, *Holography: Basic Principles and Contemporary Applications*, BoD – Books On Demand, InTech, Rejeka, Croatia, **2013**.
36. J. Persson, A. L. Mölder, S.-G. Pettersson, K. Alm, Microscopy: Science, Technology, Applications and Education. Formatex, Badajoz, Spain **2010**.
37. B. Péter, B. Majoros, S. Kurunczi, A. V. Ács, I. Szekacs, S. Bősze, G. M. Kovács, I. Boldizsár, R. Horvath, *Int. J. Biol. Macromol.* **2023**, *233*, 123528.
38. B. Peter, R. Ungai-Salanki, B. Szabó, A. G. Nagy, I. Szekacs, S. Bősze, R. Horvath, *ACS Omega* **2018**, *3*, 3882.
39. N. Orgovan, B. Kovacs, E. Farkas, B. Szabó, N. Zaytseva, Y. Fang, R. Horvath, *Appl. Phys. Lett.* **2014**, *104*, 083506.
40. J. Li, X. Zhang, H. Renata, *Angew. Chem. Int. Ed. Engl.* **2019**, *58*, 11657.
41. M. Hao, H. Xu, *Chem. – A Eur. J.* **2024**, *30*, e202302595.
42. B. Geiger, J. P. Spatz, A. D. Bershadsky, *Nat. Rev. Mol. Cell Biol.* **2009**, *10*, 21.
43. D. M. Shayakhmetov, A. M. Eberly, Z.-Y. Li, A. Lieber, *J. Virol.* **2005**, *79*, 1053.
44. J. S. Desgrosellier, D. A. Cheresh, *Nat. Rev. Cancer* **2010**, *10*, 9.
45. X. Hang, Z. Huang, S. He, Z. Wang, Z. Dong, L. Chang, *Small Methods*, **2024**, *8*, 3.

SUPPORTING INFORMATION

Additional supporting information can be found online in the Supporting Information section at the end of this article.

How to cite this article: B. Péter, T. Ausbüttel, N. Kanyo, P. Joó, K. Tóth, Z. Szittner, I. Szekacs, S. Bosze, G. M. Kovács, I. Boldizsár, R. Horvath, *VIEW.* **2025**, 20250061.
https://doi.org/10.1002/VIW.20250061